Scientific paper

Graphene Oxide/Polyamidoamine G4 as a High Efficient and Eco-Friendly Adsorbent for Dichromate Ions

Razieh Shekari Moghadam, Babak Samiey^{1,*} and Jiang Ning Wu²

¹ Department of Chemistry, Faculty of Science, Lorestan University, Khoramabad 68137-17133, Lorestan, Iran

² Department of Chemical Engineering, Toronto Metropolitan University, Toronto, Ontario, M5B 2K3, Canada

* Corresponding author: E-mail: babsamiey@yahoo.com, samiey.b@lu.ac.ir

Received: 08-04-2023

Abstract

In this study, graphene oxide/polyamidoamine G4 was used as a biocompatible nanocomposite adsorbent to adsorb dichromate ions. In alkaline solutions, dichromate ions changed to chromate ions which were not adsorbed on the surface of adsorbent. Thus, experiments were carried out in acidic and neutral water solution. Under these conditions, adsorption sites of adsorbent were protonated by primary and ternary amine groups of adsorbent shown as $-\mathrm{NH}_3^+$ and $-\mathrm{NHR}_2^+$ respectively that adsorbed dichromate ions through electrostatic interactions. Adsorption isotherms of dichromate on graphene oxide/polyamidoamine G4 were obtained under various ionic strengths, pHs and temperatures. Isotherms were analyzed by the adsorption isotherm regional analysis (ARIAN) model. The highest observed adsorption capacity of this process was 246.7 mg g⁻¹ at pH = 0 and 318 K. Tests at pH = 2 showed that this process was endothermic. Adsorption kinetic experiments were carried out under various initial dichromate concentrations, pHs, temperatures, shaking rates and ionic strengths and were analyzed by the kinetics of adsorption study in the regions with constant adsorption acceleration (KASRA) model and intraparticle diffusion, ideal-second-order (ISO) and non-ideal process of adsorption kinetics (NIPPON) equations. The four-region ARIAN and KASRA models using a series of equations can interpret thermodynamics and kinetics of interactions of adsorbent and adsorbate under different conditions, respectively. Pb²⁺, Cd²⁺, Cr³⁺ and tannic acid were separated by graphene oxide/polyamidoamine G4 from dichromate ions and the graphene oxide/polyamidoamine G4 was recycled by using an alkaline solution.

Keywords Graphene oxide/PAMAM4, ARIAN model, KASRA model, Separation

1. Introduction

The wastewater produced by industries like cosmetics, tannery, petrochemistry, paper and food factories are dangerous for life and pollution of water sources by them is considered as one of most important threats for environment. There are different chemical, physical and biological techniques for wastewater treatment and some of them are filtration, adsorption, precipitation, coagulation, ion exchange, ozonisation, aerobic and reverse osmosis which most of them are not economic and have a complex nature. Among them, adsorbents used in adsorption method are high efficient, mostly recyclable and low cost compared with other treatment methods.

Polyamidoamine (PAMAM) compounds are environment friendly dendrimers^{9,10} and some application of them are using them as drug delivery vehicles,¹¹ dendrimer-drug conjugates,¹² dendrimer/gene complexation,¹³

size adaptive dendrimer clustered nanoparticles,14 cancer gene therapy, 15 as an anti-atrophic agent, 16 anti-inflammatory and anti-thrombotic agent, 17 pulmonary drug delivery agents.¹⁸ PAMAM compounds are generally synthesized from ethylenediamine and methyl acrylamide through a divergent method. 19-22 These dendrimer structures grow outward by alternating between Michael addition reaction of the methyl acrylate molecule to amino-terof a core initiator molecule minated surface (ethylenediamine) that leads to an ester-terminated outer layer (called half-generation) and then coupling of this compound with ethylenediamine to produce an amino-terminated surface (called full-generation). In this work, the products of the subsequent syntheses were called G -0.5, G 0, G 0.5, G 1, G 1.5, G 2, G 2.5, G 3, G 3.5 and G 4 which G is an abbreviation for generation. PAMAM generation 4 (PAMAM4) like other integer or full generations is an amino-terminated PAMAM dendrimer, ²³ Fig. 1.

Fig. 1 A PAMAM4 dendrimer fragment

Graphene oxide (GO) films are two-dimensional structures which are composed from ultra-thin layers and have large surface areas. They were produced through the modified Hummer method.^{24,25} To produce GO, strong oxidizing agents, like permanganate, make oxygenated functionalities in the graphite structure and produce graphite oxide. Graphite oxide is a hydrophilic compound and can be exfoliated in water and some organic solvents by sonication²⁶ and monolayer or few-layer oxygen-functionalized flakes of GO are produced in its dispersion. In this work, GO was produced from sonication of graphite oxide in DMF and in spite of graphite oxide, GO is not toxic.²⁷ GO has applications in catalysis,²⁸ nanocompounds,²⁹ energy storage,³⁰ biomedical usages³¹ and polymer composite materials.³²

PAMAM compounds are soluble in water and organic solvents like DMF and ethanol. Thus, in this research, for using them as adsorbent, they should be immobilized on an insoluble compound like GO. In this work, a GO suspension in DMF and a solution of PAMAM4 (an amino-terminated polyamidoamine) in DMF were mixed and interactions like electrostatic and dipole-dipole interactions between amine groups of PAMAM4 and carboxyl groups of GO,²³ and hydrophobic and Van der Waals interactions between their functional groups and physical entrapment of GO nanosheets in PAMAM4 dendrimers produced graphene oxide/polyamidoamine G4 nanocomposite (abbreviated as GO/PAMAM4) which was a stable precipitate in the used temperature and pH range.

Potassium dichromate that produces dichromate (DC) ions and in this work was considered as a pollutant, is an anionic dye used as an oxidizing agent and analytical reagent in different laboratory applications, an etching material and for cleaning glassware, tannery,³³ photography and printing.³⁴

As-synthesized GO/PAMAM4 was characterized by FTIR, XRD, BET, SEM and EDS techniques Authors analyzed effects of different parameters like pH, temperature, ionic strength, shaking rate, DC concentration and time on adsorption capacity of GO/PAMAM4 for DC. Kinetics and thermodynamics of adsorption of DC on GO/PAMAM4 were studied by the KASRA and ARIAN models and ISO and NIPPON equations. Hereafter, in this work, neutral water is called water.

2. Materials and Methods

2. 1. Chemicals

Potassium dichromate ($K_2Cr_2O_7$) (>99.9%), sodium nitrate (\geq 99%), potassium permanganate (>99%), sodium chloride (>99.5%), sodium hydroxide (>98%), hydrochloric acid (37%), concentrated sulfuric acid (98%), hydrogen peroxide (30%), methanol (\geq 99.9%), ethanol (\geq 99.9%), ethylenediamine (\geq 99%), methyl acrylate (\geq 99%), N,N-dimethylformamide (DMF) (\geq 99.8%), lead nitrate (Pb(NO₃)₂) (99%), chromium nitrate (Cr(NO₃)₂.9H₂O) (99%) and cadmium nitrate (Cd(NO₃)₂.4H₂O) (98%) were purchased from Merck. Graphite powder (<20 µm) and tannic acid was purchased from Sigma-Aldrich. All chemicals were used without further purification.

2. 2. Instruments

Pore Size Micrometrics-tristar 3020 equipment (to obtain BET isotherms), Malvern Zetasizer instrument (to obtain zeta potential), PerkinElmer Frontier FTIR spectrophotometer, Rigaku D-max C III X-ray diffractometer (XRD) using Ni-filtered Cu-K α radiation (λ = 1.5406 Å), MIRA3 TESCAN instrument at 15 keV used to take FESEM (field emission scanning electron micrograph) and EDS (energy dispersive X-ray spectroscopy) spectra.

2. 3. GO Synthesis

By following the published procedure,^{35,36} graphite oxide was prepared through a modified Hummer's method.^{23,24} Then, GO was made by sonication of graphite oxide for 30 min in DMF and at room temperature.

2. 4. PAMAM4 Dendrimer Synthesis

PAMAM4 dendrimer was synthesized using methyl acrylate and ethylenediamine, based on published methods. ^{19–22} Similar to our earlier works with generation 2 of PAMAM, ^{35,36} the first synthesized PAMAM generation was named G –0.5 and after that G 0, G 0.5, G 1, G 1.5, G 2, G 2.5, G 3, G 3.5 and G 4 compounds were prepared.

2. 5. GO/PAMAM4 Synthesis

The GO/PAMAM4 was synthesized based on the procedure used for GO/PAMAM2 synthesis.^{35–37} 5 g of

PAMAM4 was dissolved in 20 ml of methanol and then was poured dropwise to a round-bottomed flask including a solution of 1 g GO in 120 ml of DMF (formerly dissolved in DMF by 25 min sonication) stirred in 600 rpm. Then, the solution was refluxed at 80 °C for 24 h. After this step, GO/PAMAM4 was separated from solution by centrifuging its solution in 6000 for 10 min. Then, 50 ml ethanol was added to GO/PAMAM4 and was centrifuged in 6000 rpm for 15 min. This step was carried out for four times.

2. 6. The XTT Cell Viability Assay of GO/ PAMAM4

The XTT cell viability assay offers a straightforward technique for assessing cellular metabolic activity as a sign of cytotoxicity of GO/PAMAM4. The succinate-tetrazolium reductase system, which is exclusive to metabolically active living cells, reduces XTT (2,3-Bis-(2-Methoxy-4-Nitro-5-Sulfophenyl)-2*H*-Tetrazolium-5-Carboxanilide), a tetrazolium derivative, into a water-soluble orange product. The quantity of live cells in the sample determines how much orange product is produced. The total amount of mitochondrial dehydrogenases in the sample decreases as the number of live cells decreases. The absorbance, which measures the quantity of orange formazan generated, directly coincides with this drop. Tumor cell lines used were Hep2, Vero cells and human hepatoma G2 (HepG2) cells.^{38,39} Details of this test were explained in Supporting Information, Fig. S1.

2. 7. Adsorption Isotherms and Kinetic Tests

Adsorption experiments were carried out by adding 10 mL of DC solutions with different initial concentrations to 0.0015 g of GO/PAMAM4. The solutions were shaken at 100 rpm in a temperature-controlled water bath shaker (Fater electronic Co., Persian Gulf model) at 308, 318 and 328 K within ± 0.1 K for 6 h to reach equilibrium. The initial concentration ranges of DC were $1\times 10^{-5}-2\times 10^{-4}$ M. After completion of adsorption, DC concentrations were measured by a UV mini 1240V Shimadzu spectrophotometer at its maximum wavelength values. The $\lambda_{\rm max}$ value of DC at pHs of 0–6 (neutral water), was 350 nm. In alkaline pHs, DC ion changed to chromate ion and its $\lambda_{\rm max}$ value was 375 nm. DC adsorption capacity on the GO/PAMAM4, q_e (mg g $^{-1}$), was calculated using the following relation

$$q_e = \frac{\left(c_0 - c_e\right)Mv}{1000 \ w} \tag{1}$$

where c_0 and c_e are the initial and equilibrium concentrations of adsorbate in each solution (M) respectively, M is the molecular weight of adsorbate (mg mole⁻¹), ν is the volume of solution (mL) and w is the weight of the used adsorbent (g).

To carry out adsorption kinetic experiments, 0.0015 g GO/PAMAM4 samples were added to 10 mL of DC solu-

tions. In this series of experiments, initial concentrations of used DC solutions were 5×10^{-5} , 1×10^{-4} and 2×10^{-4} M. These solutions were shaken at 40, 70 and 100 rpm in a temperature- controlled water bath shaker (Fater electronic Co., Persian Gulf model) at 308, 318 and 328 K and different ionic strengths and pHs. The DC residual concentrations in the solutions were measured at various contact times during the adsorption process, by a UV mini 1240V Shimadzu spectrophotometer at their values. To calculate adsorption capacity of DC on on GO/PAMAM4, q_t (mg g⁻¹), the following relation was used

$$q_t = \frac{(c_0 - c_1)Mv}{1000 w} \tag{2}$$

where c_t and q_t are adsorbate concentration (M) at time t and the adsorption capacity at time t (mg g⁻¹), respectively.

2. 8. Adsorption Isotherms and Models

Thermodynamics of adsorption was analyzed using adsorption isotherms. Adsorption isotherms were studied by the ARIAN model which is an abbreviation for "adsorption isotherm regional analysis model". All This model was introduced by Samiey and is used for analysis of adsorption isotherms up to four regions (I to IV). In this work, isotherms included regions I, II and IV, and we explained about them. A comprehensive explanation about the ARIAN model was written in Supplementary Information. The region I of the ARIAN model is studied by the Henry's law:

$$q_e = Kc_e \tag{3}$$

where there is a linear relation between adsorbate concentration and adsorption capacity and *K* is the binding constant of adsorbate on the adsorbent surface. This equation studies the most active adsorption sites. In this model, region II starts from the <u>starting second region concentration</u> (abbreviated as *ssc*) point. In region II, monolayer adsorption happens and is analyzed by an appropriate isotherm such as the Temkin equation, etc. The Temkin equation⁴² is written as

$$q_e = c_1 \ln(c_2 c_e) \tag{4}$$

where c_1 is a constant and c_2 is adsorption equilibrium constant.

The region IV of this model begins where the adsorption capacity reaches the maximum, showing a plateau on the isotherm, or where the isotherm starts to go down.⁴⁰ Here, region IV showed the maximum. Depending upon the features of adsorbate and adsorption sites, two or more sub-regions may be observed in each of regions II or III or IV of an adsorption isotherm. Each of these sub-regions are called a section and are characterized as IIA, IIB,... for the purpose of differentiation.

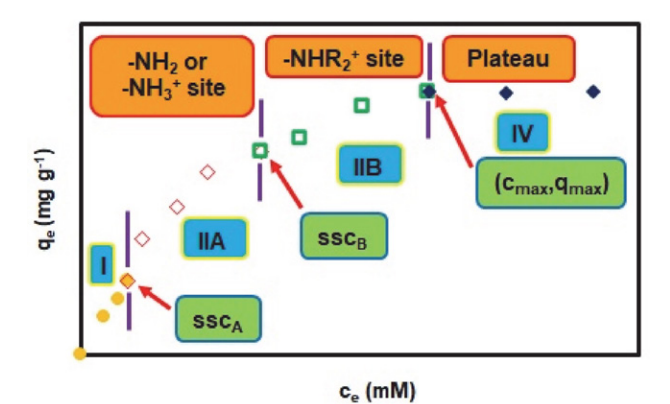


Fig. 2. Typical adsorption isotherms of DC on mesoporous adsorption sites of GO/PAMAM4 in different regions according to the ARIAN model

Typical adsorption isotherm of DC on GO/PAMAM4 based on the ARIAN model was shown in Fig. 2.

2. 9. Adsorption Kinetic Models and Equations

There are several equations for study of adsorption kinetics. The intraparticle diffusion equation⁴³ is written as

$$q_t = k_{dif} t^{0.5} + I \tag{9}$$

where k_{dif} is the rate constant for intraparticle diffusion and I is the boundary layer thickness.

The KASRA model and KASRA equation^{44–46} were used for analysis of the adsorption kinetics, too. KASRA is an abbreviation for "kinetics of adsorption study in the regions with constant adsorption acceleration". The KASRA model is based on the three assumptions for adsorption of an adsorbate species on an adsorption site: (1) each time range that adsorption acceleration in it is constant, is called a "region", (2) there are two regions before reaching the plateau region, and (3) the boundary between the first and second regions is named starting second region (abbreviated as ssr) point and that of between the second and third (plateau) regions is named kinetics of adsorption termination (abbreviated as kat) point. ssr and kat points are determined by the KASRA equation 44,45 which is given as follows:

$$q_{t} = \frac{1}{2}a_{i}t^{2} + (v_{0i} - a_{i}t_{0i})t + q_{0i} - \frac{1}{2}a_{i}t_{0i}^{2} - (v_{0i} - a_{i}t_{0i})t_{0i}$$
(10)

where q_0 , v_{0i} and t_{0i} are q_i , velocity and time at the beginning of the *ith* region, respectively and a_i is the acceleration of adsorption kinetics in the *ith* region whereas i = 1-3. Each a_i is a negative value because during adsorption process the adsorbate concentration decreases. In the first region, t_{01} and q_{01} are equal to zero. The second region begins from *ssr* point which is assigned with the coordinates t_{02} and q_{02} . Finally, plateau (third) region starts at the equi-

librium time, t_e , and equilibrium adsorption capacity, q_e which are coordinates of kat point. In this region, $v_{03} = a_3 = 0$, $t_{03} = t_e$ and $q_{03} = q_e$ and Eq. (10) is simplified to $q_t = q_e$. Due to different features of the first and second regions, parameters obtained for these two regions like rate constants are different from each other.

In this work, to avoid confusion in relation to the regions in isotherms and kinetic curves, kinetic regions are shown using numbers like region 1, etc. Typical adsorption kinetic curves of DC on GO/PAMAM4 based on the KASRA model were shown in Fig. 3.

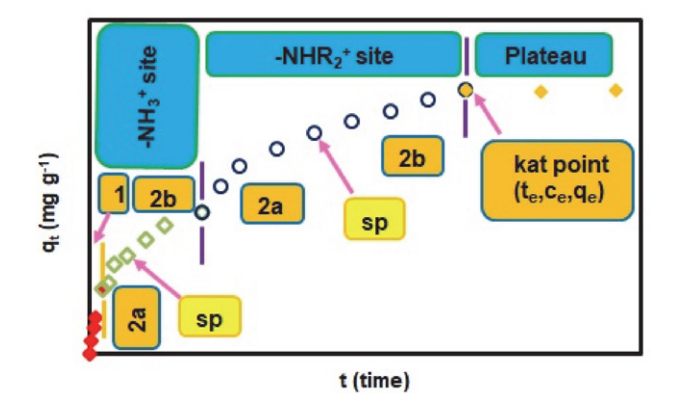


Fig. 3. Typical adsorption kinetic diagrams of DC on mesoporous adsorption sites of GO/PAMAM4 at pH=2 based on the KASRA model

The \underline{i} deal- \underline{s} econd- \underline{o} rder (or abbreviated as ISO) equation 45 is given as

$$\ln\left(\frac{q_e - q_t}{ac_t}\right) = -\frac{k_I c_e}{q_e} t + A' \tag{11}$$

where $k_I = k_I^2 q$.²⁷ k_I and k_I^2 are the first- and second-order adsorption rate constants of the ISO equation in each region and are in M⁻¹ mg g⁻¹ min⁻¹ and M⁻¹ min⁻¹, respec-

tively and
$$A' = \ln \left(\frac{q_e}{ac_o} \right)$$
 (where $a = \frac{Mv}{1000 w}$), v is the volume

of solution (ml), w is the weight of the used adsorbent (g) and M is the molecular weight of adsorbate (mg mole⁻¹).

As referred before, based on the KASRA model, there are two regions in adsorption kinetic curves before reaching the plateau which result from non-ideality in adsorption process. In the first one, completely ideal adsorption happens on the bare surface of adsorbent. The progressively changes occurred on the surface of adsorbent in region 1 finally result in emerging another ideal region (region 2) in which adsorption carries out on a partly adsorbate-covered surface. Using the ISO equation shows that region 2 is composed from two another ideal parts that are named 2a and 2b. The first part of the second region, 2a, begins after *ssr* point and the second one, 2b, starts after *starting second part* (or abbreviated as *sp*) point

and ends at the *kat* point.⁴⁴ Detailed explanation of the ARIAN model equation was written in Supporting Information.

If the ISO rate constant of a step obeys Arrhenius equation, that step is adsorption- or reaction-controlled and otherwise it is called diffusion-controlled. As referred above, in some adsorbents, there are two or more different adsorption sites which lead to observing two or more successive adsorption kinetic curves in an adsorption kinetic diagram. In these cases, region 1, (completely ideal) is only observed in the first adsorption kinetic curve, ³⁵ Fig. 3. Detailed explanation of the ISO equation was written in Supporting Information.

The NIPPON equation is used to determine the exact nature of the boundary of adjacent regions obtained from the KASRA equation.⁴⁷ The NIPPON equation is written as

$$q_t^N = k \ln(1+t) + cte \tag{12}$$

where $cte = q_{ts}^N + k \ln(1 + t_s)$. q_{ts}^N , k and t_s are adsorption capacity, rate constant and time in the starting point of the assumed time range, respectively. When $t \ll 1$ we have $\ln(1 + t) \approx t$ and then

$$q_t^N = kt (13)$$

Dimension of natural logarithm argument, 1 + t, is

in $\frac{time}{1 \text{ unit of time}}$. Equation (12) was derived and introduced

by Samiey,⁴⁷ and was called "<u>non-ideal process of adsorption</u> kinetics equation" or abbreviated as the NIPPON equation. NIPPON is a Japanese name of Japan and means the origin of sun. By taking the first and second derivatives of the NIPPON equation, non-ideal velocity and non-ideal acceleration adsorption kinetic equations, Eqs. (14) and (15), were obtained respectively. These equations are as follows

$$v_t^N = \frac{k}{1+t} \tag{14}$$

$$a_t^N = -\frac{k}{(1+t)^2} \tag{15}$$

where v_t^N and a_t^N were non-ideal velocity and acceleration of adsorption of adsorbate, respectively. On the other hand, at t = 0, $v_0^N = k$ and $a_0^N = -k$ and at $t = t_e$ we have

$$v_e^N = \lim_{l \to \infty} \frac{k}{l+t} = 0 \tag{16}$$

$$a_e^N = -\lim_{t \to \infty} \frac{k}{(1+t)^2} = 0 \tag{17}$$

where v_e^N and a_e^N were non-ideal velocity and acceleration of adsorption of adsorbate at $t = t_e$, respectively. In initial time ranges of adsorption process, adsorption is ideal and

may comply with the KASRA equation. Detailed explanation of the NIPPON equation was written in Supporting Information.

3. Results and Discussion

3. 1. Characterization of GO/PAMAM4

BET nitrogen adsorption- based isotherms were used to calculate the surface area of as-synthesized GO/PAMAM4 and DC-adsorbed GO/PAMAM4 BET samples obtained at pH = 2, Fig. S1. BET isotherms on these tests, were Type IV and based on them, GO/PAMAM4 was a porous material, Fig. S2.

Based on the BET isotherms, the BET surface area, adsorption average pore diameter (by BET) and pore volume were 17.41 m² g¹, 5.52 nm, 0.033 cm³ g¹ for as-synthesized GO/PAMAM4 and 13.33 m² g¹, 5.47 nm and 0.029 cm³ g¹ for DC-adsorbed GO/PAMAM4 at pH = 2, respectively. As reported before, 48 the surface area of GO is 9.10 m² g¹ and doubling the surface area in GO/PAMAM4 verified more exfoliation of GO layers during synthesis of GO/PAMAM4.

Data obtained from BET surface area measurements of GO/PAMAM4 showed that its pores were mesopore which involved in adsorption process. The obtained hysteresis loops of these BET isotherms were H3 which were ascribed to aggregates (loose assemblages) of platelike particles (GO layers) forming slit-like pores.⁴⁹

IR spectra of as-synthesized GO, PAMAM4 and GO/PAMAM4 compounds and GO/PAMAM4 samples were taken under various experimental conditions by using KBr pellet technique, Figs. 4(a)–4(h). In the IR spectrum of GO, peaks at 3090.0, 1727.3, 1653.8 and 1097.8 cm⁻¹ were assigned to the vibration modes of –OH, –COOH, C=O and C–O groups,⁵⁰ respectively, Fig. 4(a).

In FTIR spectrum of PAMAM4, Fig. 4(b), the peak at 3621.7 cm⁻¹ was assigned to stretching vibration modes of –OH groups of methanol impurity and 3336.5 cm⁻¹ was attributed to –NH₂ group and the peak at 1564.2 cm⁻¹ was assigned to the amide C=O group stretching vibration modes, respectively.^{23,51,52} The peaks at 2867.0 and 1488.9 cm⁻¹ were assigned to the stretching and bending vibration modes of aliphatic CH₂ group and peak at 1186.9 cm⁻¹ was attributed to ternary amine stretching vibration modes respectively.⁵¹ Lack of peak at 1740.0 cm⁻¹ assigned to carboxyl C=O group proposed formation of PAMAM4 from its 3.5 half generation

FTIR spectrum of GO/PAMAM4 showed peaks at 1560.0 cm⁻¹ (assigned to –CONH– of PAMAM4), 2839 cm⁻¹ (attributed to aliphatic CH₂ group of PAMAM4)⁵³ and 3209.5 cm⁻¹ (assigned to –OH group of GO) confirmed that the PAMAM4 was grafted onto the flakes of GO, Fig. 4(c). This information showed that GO/PAMAM4 was synthesized successfully.

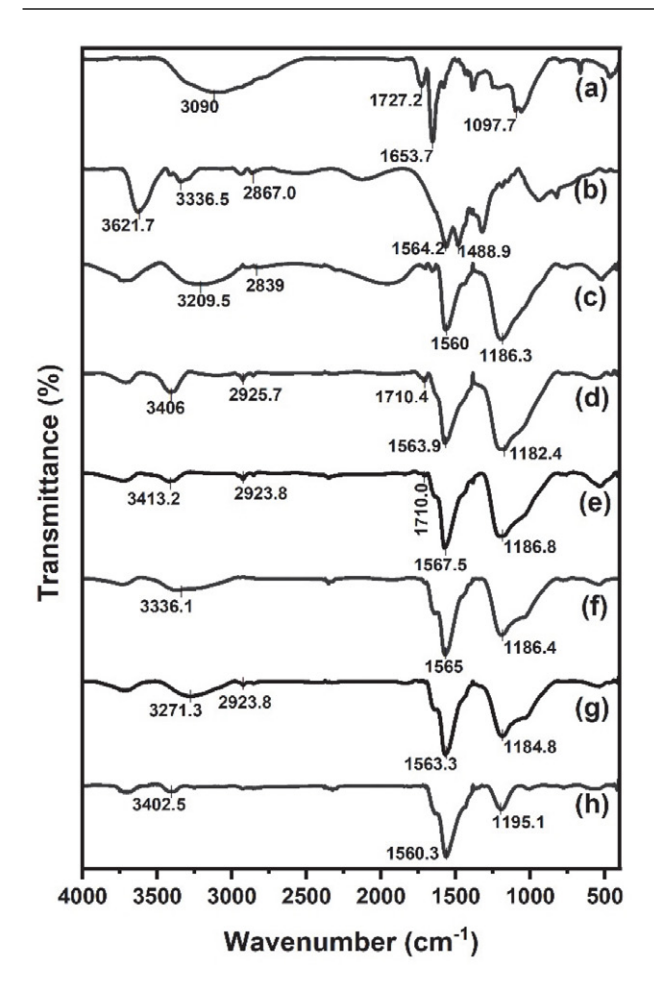


Fig. 4. IR spectra of (a) as-synthesized GO, (b) PAMAM4, (c) GO/PAMAM4 and DC-adsorbed GO/PAMAM4 samples at pHs of (d) 1, (e) 2, (f) 3, (g) 6 (water) and (h) 11

Peaks of –NH– part of amide groups in FTIR spectra of DC-adsorbed GO/PAMAM4 at pHs of 1, 2, 3, water and 11 appeared at 1563.9, 1567.5, 1565.0, 1563.3 and 1560.3

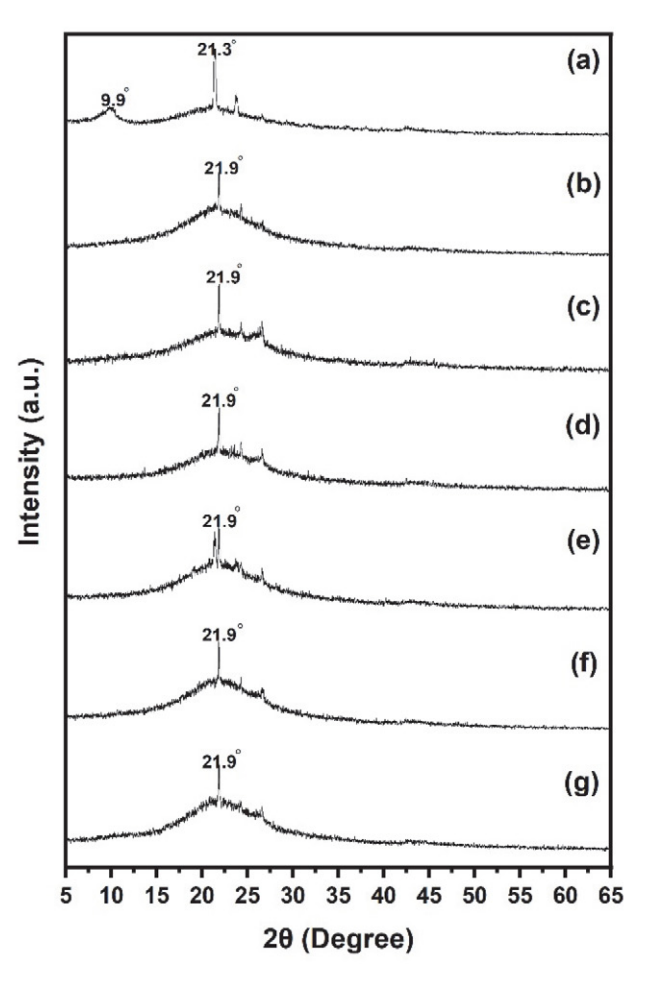
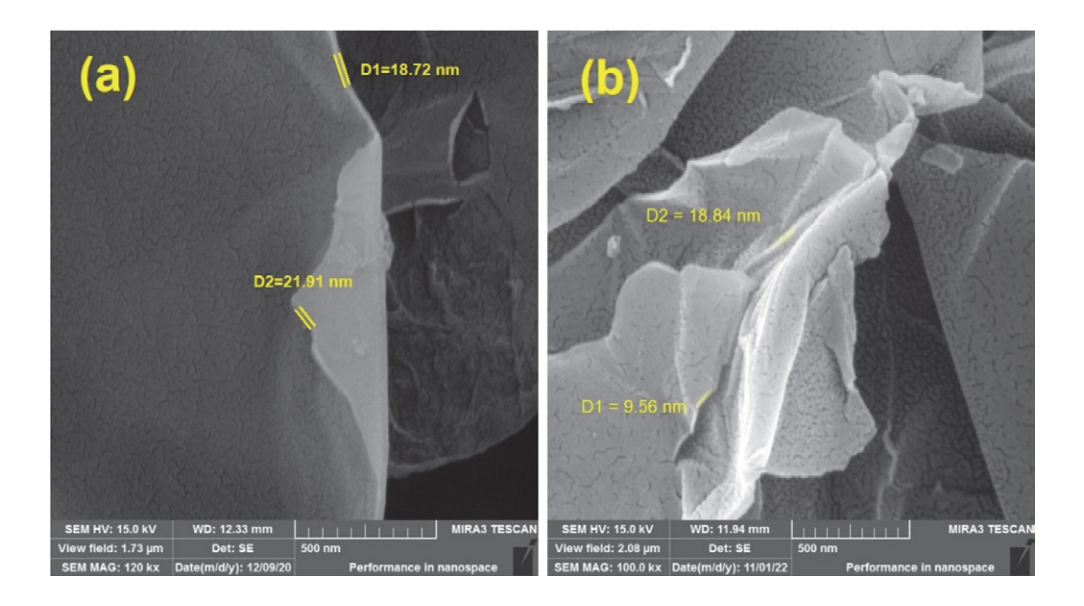


Fig. 5. XRD spectra of (a) as-synthesized GO, (b) as-synthesized GO/PAMAM4 and DC-adsorbed GO/PAMAM4 samples at pHs of (c) 1, (d) 2, (e) 3, (f) 6 (water) and (g) 11

cm⁻¹ were approximately similar to those of as-synthesized GO/PAMAM4 that confirmed that -NH- part of their amide groups didn't interact with DC ions, Figs.



Moghadam et al.: Graphene Oxide/Polyamidoamine G4 as a High Efficient ...

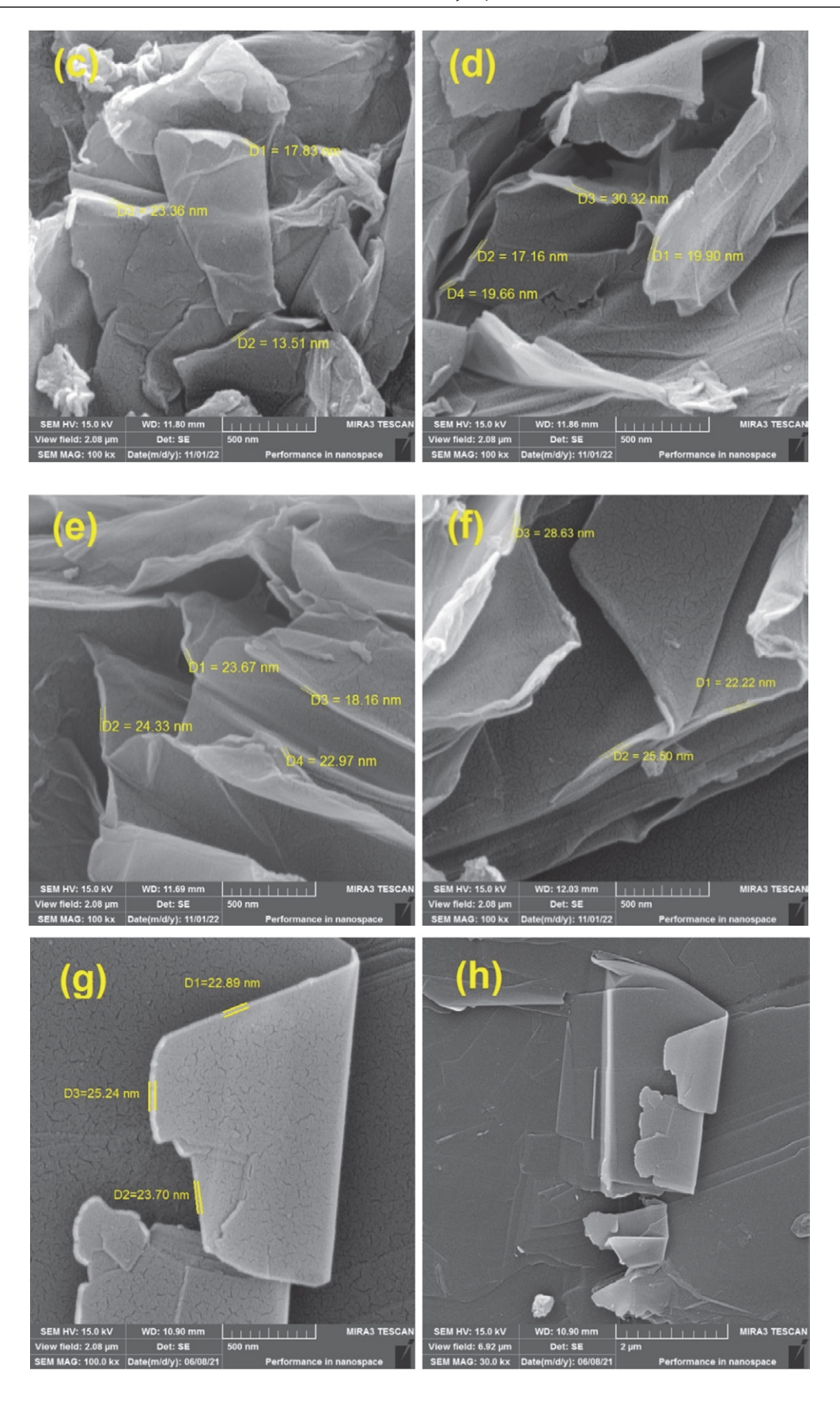


Fig. 6. FESEM images of (a) pristine GO/PAMAM4 and DC-adsorbed GO/PAMAM4 at pHs of (b) 1, (c) 2, (d) 3, (e) 6 (water), (f) 11, (g) and (h) GO. The magnification of the SEM images from (a) to (g) is 100,000 x and that of (h) is 30,000 x

4(d)–4(g) which was due to their involvement in resonance forms of amide group. Also, as seen in Figs. 4(c)–4(g), the IR spectra of the adsorbent in the pH range of 1–11 were very similar to each other that confirmed that the GO/PAMAM4 was stable in the pH range of 1–11 in the presence of DC.

Crystalline structure of as-synthesized GO, GO/ PAMAM4 and GO/PAMAM4 and several DC-adsorbed GO/PAMAM4 samples were obtained under different experimental conditions, Figs. 5(a)-5(g). The weak peak of as-synthesized GO at 2θ of 9.9° was attributed to (002) crystal planes⁵⁴ and broad peak appeared at 2θ of 21.3° was attributed to amorphous GO,53 Fig. 5(a). Broad peak of pristine GO/PAMAM4 and DC-adsorbed GO/PAMAM4 samples at 20 of 21.9° was assigned again to the amorphous exfoliated structure of graphitic layers of its GO part and peak observed at 2θ of 9.9° of its GO part disappeared due to its exfoliation after interaction with PAMAM4 dendrimer, Figs. 5(b)-5(g). Peaks of XRD spectra of DC-adsorbed GO/PAMAM4 at pHs of 1, 2, 3, water and 11 appeared at 2θs of 21.9° and were similar to each other which confirmed that GO/PAMAM4 structure was stable under used conditions, Figs. 5(b)-5(g).

Images of as-synthesized GO/PAMAM4 and its samples were taken at various pHs, Figs. 6(a)-6(h) and Fig. S3. It was shown that average thickness of GO was 23.94 nm, Fig. 6(h) and that of PAMAM4-covered GO layers in pristine GO/PAMAM4 was 20.32 nm which confirmed that GO/PAMAM4 was a two-dimensional nanocompound, Fig. 6(a). Decrease in thickness of GO layers of GO/ PAMAM4 and change in morphology and decrease in glossiness of GO/PAMAM4 layers, Fig. 6(a), compared to those of GO, Fig. 6(h), verified formation of GO/PAMAM4. It was observed that PAMAM4 dendrimers surrounded GO nanosheets surface and GO/PAMAM4 was formed through electrostatic, dipole-dipole and Van der Waals interactions between their functional groups.²³ Also, as seen in Figs. 6(a)-6(f), morphologies of GO/PAMAM4 in the pH range of 1-11 were similar to each other.

EDS (energy dispersive X-ray spectroscopy) spectra of pristine GO, pristine GO/PAMAM4 and DC-adsorbed GO/PAMAM4 samples were taken under different experimental pHs and confirmed that DC ions did not adsorb on GO/PAMAM at pHs upper than 6, Table 1.

Also, it was observed that treatment of Hep2, HepG2 and Vero cells with GO/PAMAM4 in XTT assay had no toxic effect on the cells compared to the control group and showed that GO/PAMAM4 was an eco-friendly compound, Supporting Information, Fig. S1.

Information obtained from IR, XRD, SEM, EDS and BET techniques verified synthesis of GO/PAMAM4 nanocompound.

3. 2. Adsorption Isotherms of DC on GO/ PAMAM4

As seen in Fig. 7, DC ions were changed to chromate ions in pHs higher than 6 (water) and our investigation showed that adsorption on the surface of GO/PAMAM4 happened till pH of 6. It confirmed that only DC ions were adsorbed on the surface of GO/PAMAM4. Adsorption isotherms of this process were studied by the ARIAN model at 308–328 K, various ionic strengths and pHs, Tables 2 and 3 and Fig. 8.

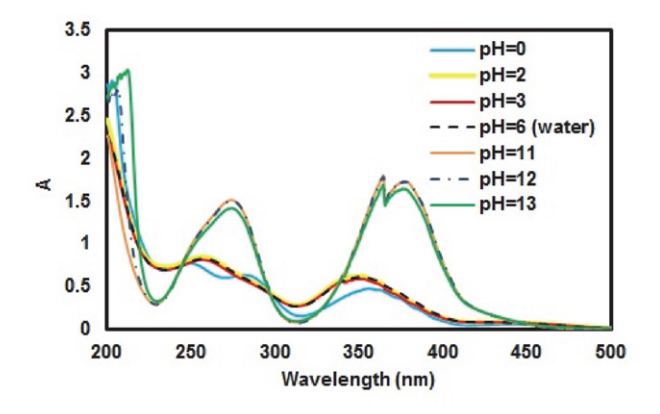


Fig. 7. UV-Vis spectra of DC at pHs of 0, 2, 3 and 6 and those of chromate ions at pHs of 11, 12 and 13 at room temperature. All tests were carried out using 0.2 mM solutions of

As referred before, Figs. 3(c)–3(g), amide groups of GO/PAMAM4, due to formation of resonance forms and involvement of their –NH– part in these forms did not interact with DC ions at pH range of 1–6.

In neutral aqueous (pH \approx 6) and pH = 3 solutions of DC ions, only acidic form of primary amine groups of GO/

 $\textbf{Table 1.} \ Elements \ weight percentage \ (W\%) \ of \ as-synthesized \ GO/PAMAM4 \ and \ DC-adsorbed \ GO/PAMAM4 \ samples \ under various \ pH \ conditions \ obtained \ from \ their \ EDS \ spectra$

Element	GO	As-synthesized			DC-a	dsorbed G	O/PAMAM	4 at	
		GO/PAMAM4	pH = 1	pH = 2	pH = 3	water	pH = 11	pH = 12	pH = 13
С	82.3	61.2	54.5	62.5	55.3	64.4	64.2	62.9	60.1
N	_	14.3	21.4	16.9	22.1	17.9	20.6	21.2	22.1
O	17.7	24.5	19.5	18.5	21.2	17.3	14.7	15.1	16.6
Cl	_	_	4.1	1.4	0.9	_	_	_	_
Cr	_	_	0.5	0.7	0.5	0.4	_	_	_
Na	-	-	-	_		_	0.5	0.8	1.2

Table 2. Parameters obtained from the Henry and Temkin isotherms of different regions (I and II) and ssc_A , q_{sscA} , ssc_B and q_{sscB} values for adsorption of DC on GO/PAMAM4 in water, acidic and alkaline solutions at 308–328 K

Solvent	\boldsymbol{T}	Hei	nry (regio	n I)	Teml	cin (section	ı IIA)	Temk	in (sectio	n IIB)
	(K)	K	ssc _A	q_{sscA}	c_2	ssc _B	q_{sscB}	c_2	c _{max}	q _{e,max}
		DC	on -NH ₃	site	DC	on –NH ₃	site	DC	on –NHR	site
pH = 0	318	2.06×10^{6}	0.016	46.8	1.02×10^{5}	0.029	100.1	5.66×10^4	0.074	246.7
pH = 1	318	5.58×10^{6}	0.010	58.6	2.36×10^{5}	0.039	159.1	2.07×10^{5}	0.075	206.2
pH = 2	308	4.09×10^{6}	0.010	39.8	2.66×10^{5}	0.034	89.7	1.05×10^{5}	0.095	165.2
•	318	6.95×10^{6}	0.006	46.0	3.44×10^{5}	0.021	114.7	2.22×10^{5}	0.086	222.6
	328	2.44×10^7	0.003	72.5	1.91×10^{6}	0.013	131.6	3.69×10^{5}	0.056	242.7
0.1 M NaCl	318	1.20×10^{6}	0.037	45.1	5.26×10^4	0.073	92.9	2.87×10^{4}	0.121	154.9
pH = 3	318	3.43×10^{6}	0.015	50.1	9.87×10^{5}	0.028	119.8	_	_	_
Water	318	6.55×10^{5}	0.066	45.0	2.14×10^4	0.014	141.1	_	_	_

Units of K and c_2 are in mg g⁻¹ M⁻¹ and M⁻¹, respectively. Units of ssc_A , ssc_B and c_{max} are in mM. Units of q_{sscA} , q_{sscB} and $q_{e,max}$ are in mg g⁻¹. At pHs of 2 (in 0.1 M NaCl), 3 and water, due to lack of section IIB, section IIA is region II and $q_{sscB} = q_{e,max}$ and $ssc_B = c_{max}$.

Table 3. Equilibrium constants (K) and thermodynamic parameters for adsorption of DC on GO/PAMAM4 in water and at pH = 2 solutions at 308–328 K

pН	308 K	318 K	328 K	ΔΗ	ΔS
	K ΔG	K ΔG	K ΔG		
2 (region I)	4.09×10 ⁶ -39.0	6.95×10 ⁶ -40.3	2.44×10 ⁷ -43.6	74.7	367.9
2 (section IIA)	$2.66 \times 10^5 -32.0$	3.44×10^5 -32.6	1.91×10^6 -37.0	82.1	368.4
2 (section IIB)	1.05×10^5 -29.6	2.22×10^5 -31.5	$3.69 \times 10^5 -32.8$	52.9	268.0

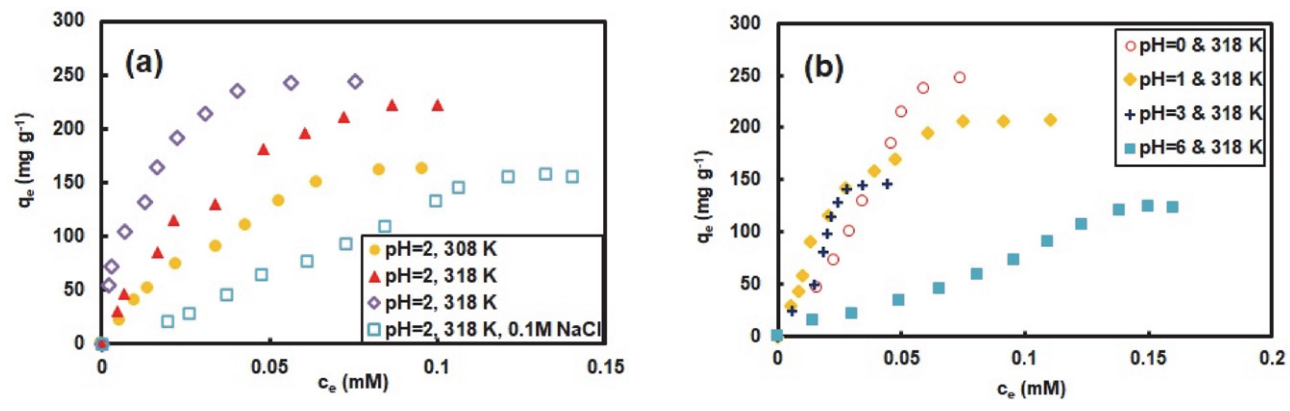


Fig. 8. Adsorption isotherms of DC on GOPAMAM4 (a) at pH = 2 and at ● 308 K, ▲ 318 K, ♦ 328 K and □ in 0.1 M NaCl at 318 K and (b) at pHs of ○ 0, ◆ 1, + 3 and ■ 6 (water) at 318 K. All tests were carried out at 100 rpm

PAMAM4, -NH₃⁺ groups, are its adsorption sites for DC ions. Hydrogen atom of these groups interact with oxygen atom of DC ions. Analysis of adsorption isotherms at these pHs by the ARIAN model showed that they were formed from regions I and II which were studied by the Henry and Temkin isotherms, respectively, Table 2.

At each pH value, due to steric hindrance of adsorbed molecules and an increase in negative charge of adsorbent surface, adsorption equilibrium constants decreased from region I to region II. As reported before, PAMAM generations are positively charged at water⁵⁵ and adsorbent surface potential became more positive with a decrease in pH of solutions.⁵⁶ As measured at this work,

pH of point of zero charge (pH $_{PZC}$) of GO/PAMAM4 was 3.9 and a decrease in pHs of DC solutions from pH of 6 (water) to 3 made more positive the surface potential of GO/PAMAM4, Fig. 9 and resulted in an increase in adsorption equilibrium constants in regions I and II of process at pH of 3 compared to that at pH of 6. On the other hand, this caused stronger interactions between these protonated ternary amine and amide groups of PAMAM4 dendrimers which made its structure more compact and decreased adsorbent capacity. 36,57,58

At pH = 2, due to the repulsion between primary and tertiary amines of PAMAM4 dendrimer, its structure was opened⁵⁹ and as observed, $-NR_2H^+$ groups could adsorb

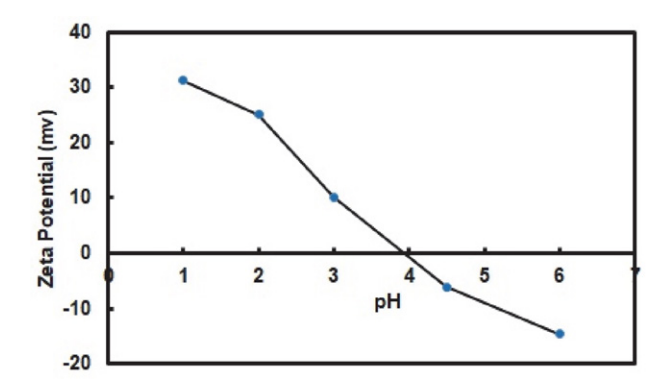


Fig. 9. Zeta potential vs. pH for GO/PAMAM4

DC ions. Due to steric hindrance of big R groups of $-NR_2H^+$ groups, lower tendency for attachment to proton and more hydrophobicity character of ternary amines compared to primary amines, electrostatic interactions of DC ions with $-NR_2H^+$ groups (region I) were weaker than that with $-NH_3^+$ groups (region II) of adsorbent, Table 2.

At this pH, isotherms were composed from regions I and section IIA for adsorption of DC ions on $-NH_3^+$ and section IIB for adsorption of DC ions on $-NR_2H^+$ adsorption sites, respectively. The adsorption processes in all these three regions were endothermic that was due to hydrophobic interactions of DC ions with opened adsorbent structure and their entropy changes were large positive numbers

which was due to disorder in the adsorbent structure and detaching water molecules from adsorption sites during adsorption process, Table 3. In 0.1 M NaCl solutions of DC at pH = 2 and 318 K, the equilibrium adsorption constants and adsorption capacity of this adsorption process decreased compared to their values at pH = 2 and 318 K which was due to surrounding effect of Na $^+$ ions on DC ions.

Like pH = 2, at pHs of 0 and 1, DC ions interacted with $-NH_3^+$ (analyzed by the Henry and Temkin isotherms) and $-NR_2H^+$ (analyzed by the Temkin isotherm) groups of adsorbent and adsorption capacities of DC ions on GO/PAMAM4 decreased with a decrease in pH from 2 to 1, due to formation of $HCr_2O_7^-$ from a number of DC ions (pKa = $1.18)^{60}$ and increased with a decrease in pH from 1 to 0 which was due to a highly increase in positive charge of adsorbent surface⁵⁹, Fig. 9. Mechanism of adsorption of DC on GO/PAMAM4 in different pH ranges was shown in Fig. 10.

As seen from XRD and IR spectra and SEM images of pristine GO/PAMAM4 and DC-adsorbed GO/PAMAM4 at different pHs, structure of adsorbent is stable under different conditions in these series of tests, Figs. 4–6.

At the end, adsorption capacities of a number of adsorbents for potassium dichromate were shown in Table 4 and as it is evident, adsorption capacity of GO/PAMAM4 for DC is higher than most of other adsorbents used for this purpose. 61–67

Table 4. Maximum adsorption capacity $(q_{e,max})$ of DC on a number of compounds

Adsorbent	pН	T (K)	$q_{e,max}$ (mg g ⁻¹)	Reference
Graphene oxide-magnetic	2	298	3.2	61
Carboxyl-rich carbon nanocomposite	1	298	142.9	62
Zr ⁴⁺ cross-linked magnetic chitosan/polyaniline composite	2	298	491.4	63
MCM-41-AEAPTMS-Fe(III)Cl	3	298	84.9	64
Meidum black clay and pomegranate peel extract	2	323	78.1	65
Mag@LDH-ER	7	298	54.7	66
Chitosan	5	298	7.4	67
GO/PAMAM4	0	318	246.7	This work

Fig. 10. Schematic representation of adsorption of DC on GO/PAMAM4 in different pH ranges

3. 3. Adsorption Kinetics of DC on GO/ PAMAM4

Kinetics of DC adsorption on GO/PAMAM4 surface was studied in different initial DC concentrations, temperatures, ionic strengths, shaking rates and pHs. Kinetic curves were analyzed by the KASRA model and ISO, intraparticle diffusion and NIPPON equations, as given in Figs. 11 and 12 and Tables 5–7. Analysis of the kinetic curves by the KASRA model and intraparticle diffusion equation showed that they were composed from one or two curves and in each curve there were two regions (1 and 2) and their accelerations and velocities of adsorption and k_{dif} values decreased from region 1 to region 2. This is due to a decrease in DC concentration and an increase in negative charge of adsorbent surface and spatial hindrance on adsorption sites due to adsorbed DC ions.

As referred before, at pH = 6 (neutral aqueous solutions) and pH = 3 DC solutions, $-NH_3^+$ groups of GO/PAMAM4 adsorbed DC ions. In each of these cases, the initial DC concentration was 0.2 mM which was on the plateau of their isotherm and was involved all interactions between

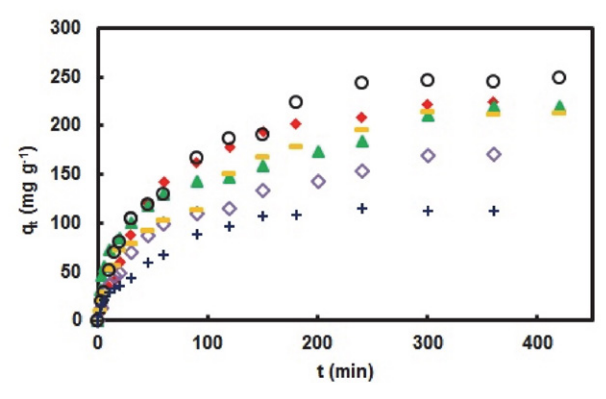


Fig. 11. Adsorption kinetic curves of DC on GOPAMAM4 at pHs of \spadesuit 0, \spadesuit 1 and + 3 at 318 K and at pH = 2 at \diamondsuit 308, – 318 and \bigcirc 328 K. All tests were carried out at 100 rpm and in [DC] $_0$ = 0.2 mM

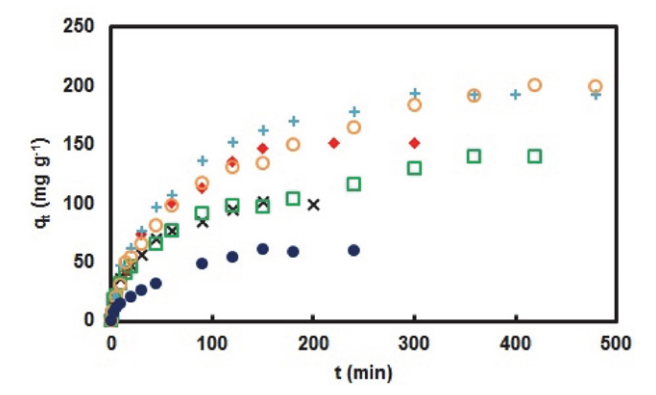


Fig. 12. Adsorption kinetic curves of DC on GOPAMAM4 \spadesuit at pH = 6 and in [DC] $_0$ = 0.2 mM and 100 rpm and \Box pH = 2 in 0.1 M NaCl and [DC] $_0$ = 0.2 mM and 100 rpm and + at pH = 2, 70 rpm and in [DC] $_0$ = 0.2 mM and \bigcirc at pH = 2, 40 rpm and in [DC] $_0$ = 0.2 mM and \spadesuit at pH = 2, in [DC] $_0$ = 0.05 mM and 100 rpm and × at pH = 2, in [DC] $_0$ = 0.1 mM and 100 rpm

Table 5. Experimental $t_e, q_e, t_0, q_{0.5}, t_{0.5}$ and $q_{0.3}$ values and coefficients obtained from the KASRA equation and k_{dd} values of intraparticle diffusion equation for kinetics of DC adsorption on GO/PAMAM4 at different temperatures and in various shaking rates and initial DC concentrations

Solvent	T	[DC] ₀	rpm	KASR	KASRA region 1 (1	(1st curve)	KASR	KASRA region 2 (1st curve)	(1st curve		KASRA	KASRA region 2 (2nd curve)	2nd curv	(e)	(t_o, q_e)
	(<u>K</u>	(mM)		a_1	ν_{01}	k_{dif}	(t_{02},q_{02})	a_2	v_{02}	k_{dif}	(t_{03},q_{03})	a_3	v_{03}	k_{dif}	
Corresponding to:	ling to:			ARIAN region I		-NH ⁺ ₃ site)	ARIAN	ARIAN section IIA (-NH ⁺ ₃ site)	۱ (-NH ₃ s	ite)	RIAN Se	RIAN section IIB (-NHR ⁺ ₂ site)	(-NHR2 s	site)	
pH = 0	318	0.20	100	-0.290	5.00	13.3	(5,41.9)	-0.054	3.42	26.2	(60,142.6)	-0.002	0.84	8.6	(360,224.7)
pH = 1	318	0.20	100	-5.110	23.60	5.1	(5,55.0)	-0.018	1.80	31.4	(120,146.6)	-0.001	0.43	8.59	(480,228.7)
pH = 2	318	0.05	100	-0.100	2.54	8.1	(5,11.0)	-0.004	09.0	5.2	ı	ı	ı	1	(150,60.4)
	318	0.10	100	-0.252	4.80	12.5	(20,47.1)	-0.005	0.73	8.9	(150,101.4)	-0.001	0.34	0.9	(420,142.7)
	308	0.20	100	-0.296	5.31	12.1	(20,48.6)	-0.086	3.44	17.0	(45,86.9)	-0.001	0.45	8.9	(420,177.6)
	318	0.20	100	-0.314	6.71	21.3	(10,52.4)	-0.018	1.46	10.1	(90,114.4)	-0.004	0.79	9.5	(360,210.8)
	328	0.20	100	-0.920	7.98	17.1	(5,28.4)	-0.074	3.05	18.7	(60,130.3)	-0.003	0.91	14.4	(240,244.0)
	318	0.20	70	-0.240	5.82	19.8	(10,47.2)	-0.010	1.47	13.8	(90,136.1)	-0.001	0.40	6.9	(300, 193.6)
	318	0.20	40	-0.124	3.93	14.7	(20,54.0)	-0.009	1.23	10.9	(150,134.2)	-0.001	0.39	8.0	(420,200.6)
0.1 M NaCl	318	0.20	100	-0.200	4.24	12.4	(15,40.2)	-0.008	0.99	11.1	(150,97.4)	-0.001	0.28	11.1	(480,141.8)
pH = 3	318	0.20	100	-0.65	5.97	69.6	(15,9.69)	-0.006	1.05	9.13	I	ı	ı	ı	(240,114.5)
Water	318	0.20	100	-0.438	6.12	10.6	(15,42.5)	-0.007	1.22	12.2	I	I	I	ı	(150,147.5)
- J T I	-		-12	TT.:	1	-	-1 **	1,		1.4				-	, , , , , , , , , , , , , , , , , , , ,

Units of a_1 , a_2 and a_3 are in $\operatorname{mg} \operatorname{g}^{-1} \operatorname{min}^{-2}$ and $\operatorname{those} \operatorname{of} \nu_{01}$, v_{02} and v_{03} are in $\operatorname{mg} \operatorname{g}^{-1} \operatorname{min}^{-1}$. Units of t_c , t_{02} and t_{03} are in $\operatorname{mg} \operatorname{g}^{-1} \operatorname{min}^{-2}$ and t_{03} are in $\operatorname{mg} \operatorname{g}^{-1} \operatorname{In} \operatorname{in}^{-1}$. In region 1, t_{01} and q_{01} are equal to zero. t_c and q_e are the kat point coordinates. k_{dif} is in mg g⁻¹ min^{-0.5}.

Table 6 Coefficients of region 1 and region 2 (parts 2a and 2b) of the first kinetic curve and region 2 (parts 2a and 2b) of the second kinetic curve of the ISO equation for kinetics of DC adsorption on different sites of GO/PAMAM4 at different temperatures and in various shaking rates and initial DC concentrations

				KASRA re	KASRA region 1 (1st curve)		KASRA region 2 (1st curve)	gion 2 (1st	curve)		KASRA region 2 (2nd curve)	on 2 (2nd	curve)
Solvent	T (X)	[DC] ₀ (mM)	rpm	k_{Π}	$\frac{(t_{sr},q_{sr})}{(min,mgg^{-1})}$	k _{12a} ($\frac{(t_p,q_p)}{(min,mgg^{-1})}$	k_{12b}	$([\mathrm{DC}]_{t,max}^{1}, t^{1}, q_{t,max}^{1})$ (mM,min,mg g ⁻¹)	k_{12a} ($\frac{(t_{sp}, q_{sp})}{(\min, \operatorname{mg} \operatorname{g}^{-1})}$	k_{12b}	$([\mathrm{DC}]_e, t_e, q_e)$ (mM,min,mg g ⁻¹)
	Cor	Corresponding to:	ing to:		ARIAN reg	jon I and se	ARIAN region I and section IIA (-NH3 site)	NH ₃ site)			ARIAN	section II	ARIAN section IIB (-NHR ⁺ ₂ site)
0 = Hd	318	0.20	100	2.28×10^4	(5,41.9)	ı	ı	4.86×10^{4}	(0.127,60,142.6)	2.08×10^4	ı	1	(0.090,360,224.7)
pH = 1	318	0.20	100	2.14×10^4	(60,130.3)	ı	ı	4.46×10^4	(0.125,120,146.6)	1.04×10^4	1.04×10^4 (240,184.6) 2.26×10^4	2.26×10^4	(0.083,480,228.7)
pH = 2	318	0.02	100	1.10×10^{5}	(5,11.0)	2.17×10^4	ı	ı	(0.034,45,31.6)	3.87×10^{4}	ı	I	(0.192,150,60.4)
1	318	0.10	100	4.26×10^{4}	(20,47.1)	3.19×10^{4}	(60,77.1)	3.67×10^{4}	(0.048, 150, 101.4)	5.35×10^{4}	ı	ı	(0.029, 360, 140.9)
	308	0.20	100	2.25×10^4	(15,48.6)	ı	ı	3.17×10^{4}	(0.160, 30, 70.3)	9.04×10^{3}	9.04×10^3 (240,154.0)	2.63×10^4	(0.110,420,177.6)
	318	0.20	100	3.48×10^4	(10,52.4)	2.56×10^4	ı	ı	(0.142,90,114.4)	1.98×10^4	1.98×10^4 (180,178.2)	2.38×10^4	(0.091,300,214.0)
	328	0.20	100	3.83×10^{4}	(5,28.4)	I	I	4.49×10^4	(0.134,60,130.3)	1.97×10^{4}	$1.97 \times 10^4 \ (150,191.0)$	1.01×10^{5}	(0.076,240,244.0)
	318	0.20	20	3.18×10^{4}	(10,47.2)	$1.88{\times}10^{4}$	ı	ı	(0.131,90,136.1)	1.44×10^4	ı	ı	(0.010,300,193.6)
	318	0.20	40	1.90×10^{4}	(20,54.0)	1.67×10^{4}	(60,98.4)	3.58×10^{4}	(0.132,150,134.2)	1.70×10^4	I	ı	(0.098,420,200.6)
0.1 M NaCl	318	0.20	100	1.85×10^{4}	(20,45.9)	1.32×10^{4}	(60,76.9)	2.68×10^4	(0.150,150,97.4)	6.09×10^{3}	6.09×10^3 (240,116.4)	2.22×10^4	(0.128,480,141.8)
pH = 3	318	0.20	100	6.69×10^{4}	(5,21.4)	1.51×10^{4}	(45,59.6)	3.91×10^{4}	ı	ı	ı	ı	(0.042,240,114.5)
Water	318	0.20	100	1.70×10^4	(15,42.5)	1.37×10^4	$(90,112.7)$ 3.98×10^4	3.98×10^{4}	I	I	ı	ı	(0.125,150,147.5)

considered as the kat point coordinates. [DC]_e, t_e and q_e are DC concentration, time and adsorption capacity at the beginning of the plateau for adsorption on -NHR² sites (in the second curve), respectively and are the *kat* point coordinates, too. Units of k_{I1} , k_{I2a} , and k_{I2b} are in mg g⁻¹ M⁻¹ min⁻¹ surface of adsorbent and DC ions. As referred before, with a decrease in pH from 6 (in water) to less than 4, tertiary amine groups of PAMAM4 started to be protonated and this made adsorbent surface more positive that increased ISO kinetic parameters in regions 1 and 2 (including k_{I1} , k_{I2a} and k_{I2b}). ISO kinetic parameters are related to interaction of adsorbent surface and DC ions in the Stern layer. On the other hand, this caused stronger interactions between these protonated ternary amine groups with amide groups of PAMAM4 dendrimers which made its structure more compact and increased the time of reaching to equilibrium.

Due to surrounding effect of H⁺ ions on DC ions at pH = 3, adsorption accelerations, velocities and k_{dif} related to moving DC ions toward the Gouy layer, at this pH were less than those at pH = 6.

As referred before, due to opening the structure of PAMAM4 part of adsorbent at pHs of 0, 1 and 2, in addition to $-\mathrm{NH_3^+}$ groups of PAMAM4 as regions 1 and 2a and/or 2b in the first kinetic curve, internal $-\mathrm{NHR_2^+}$ groups of PAMAM4 as region 2a and/or 2b in the second kinetic curve involved in adsorption process. As seen from Tables 5–7, adsorption acceleration and velocities, k_{dif} and k_{I1} of region 1 increased with an increase in temperature from 308 to 328 K at 100 rpm and increasing shaking rate from 40 to 100 rpm at 318 K at 0.2 mM of DC and an increase in DC concentration from 0.05 to 0.2 mM of DC at 100 rpm and 318 K.

It was observed that only k_{I1} parameters of 0.2 mM of DC solution at 318–328 K and 100 rpm and pH of 2 obey from Arrhenius equation and their activation energy of adsorption was 22.5 kJ mol⁻¹. It showed that adsorption of DC ions on GO/PAMAM4 under these conditions was adsorption-controlled in region 1 and thus in other regions of the first and second curves was diffusion-controlled.

At pH = 1, the time of reaching to equilibrium was much greater than that observed for pHs of 0 and 2 which was due to changing some of DC ions to of HCr₂O₇ ions.⁶⁰ At pH = 0 compared to pH = 1, in region 1, adsorption accelerations and velocities decreased and ISO equation k_{I1} rate constant of adsorption increased due to an increase in positively charged adsorbent surface.

At pH = 2 and 0.1 M of NaCl, adsorption accelerations and velocities and ISO equation k_{I1} rate constant of adsorption of region 1 decreased compared to those at pHs of 1 (0.1 M of HCl) and 2 (0.01 M of HCl) at 318 K and 100 rpm which confirmed that surrounding DC ions by Na⁺ ions was responsible for these observations.

Finally, kinetic data were analyzed with the NIPPON equation and compared to regions obtained from the KAS-RA model. As seen from Table 7, there are at most three curves which can be considered correspondence to regions obtained from the KASRA model in Table 5. As seen from Table 7, based on the NIPPON equation, the boundaries of different regions of kinetic curve(s) at pHs of 1, 3 and 6 (water) and also cases at pH of 2 and 0.2 mM of DC at 318 and 328 K at 100 rpm and 318 K at 40 rpm were ideal and similar to those obtained from the KASRA model.

Table 7. Non-ideal adsorption acceleration and velocity parameters for the NIPPON curves from analysis of adsorption of DC on GO/PAMAM4 at different temperatures, various pHs, shaking rates and in various initial DC concentration

Solvent	T	$[DC]_0$	rpm	First N	IPPON	curve		Seco	nd NIPl	PON curve	Thi	rd NIPPON	V curve
	(K)	(mM)		a_{fc}^N	v_{fc}^N	t_{sc}	q_{sc}	a_{sc}^N	v_{sc}^N	t_{tc}	q_{tc}	a_{tc}^N	v_{tc}^N
pH = 0	318	0.20	100	-15.65	15.65	15	41.9	-0.03	4.67	45	121.2	-0.03	1.15
pH = 1	318	0.20	100	-30.04	30.04	10	72.6	-0.28	3.07	120	146.6	-0.004	0.51
pH = 2	318	0.05	100	-6.64	6.64	20	20.1	-0.05	0.98	_	_	_	_
•	318	0.10	100	-12.39	12.39	5	21.3	-0.62	3.96	90	85.0	-0.005	0.48
	308	0.20	100	-16.81	16.81	20	48.6	-0.09	1.83	120	115.6	-0.003	0.41
	318	0.20	100	-16.04	16.04	5	28.7	-0.86	5.18	90	114.4	-0.01	0.86
	328	0.20	100	-21.20	21.20	5	28.4	-0.04	1.26	60	130.3	-0.02	1.33
	318	0.20	70	-13.87	13.87	6	24.6	-0.98	5.85	60	106.7	-0.01	0.84
	318	0.20	40	-12.87	12.87	10	30.7	-0.33	3.68	150	134.2	-0.003	0.43
0.1 M NaCl	318	0.20	100	-15.67	15.67	20	45.9	-0.07	1.50	_	_	_	_
pH = 3	318	0.20	100	-12.84	12.84	30	43.4	-0.04	1.17	_	_	_	_
Water	318	0.20	100	-15.17	15.17	15	42.5	-0.18	2.83	_	-	_	_

Units of a_{fc}^N , a_{sc}^N and a_{tc}^N were in mg g⁻¹ hour⁻², v_{fc}^N , v_{sc}^N and v_{tc}^N were in mg g⁻¹ hour⁻¹ and t_{sc} and t_{tc} were in min and q_{sc} and q_{tc} were in mg g⁻¹, respectively. Subscripts fc, sc and tc are abbreviations for starting first, second and third curves, respectively.

At pH = 0, a small movement was observed in boundaries of regions 1 and 2 in first curve and between the first and second curves obtained from the KASRA model.

Boundary between regions 1 and 2 of the only curve in 0.05 mM of DC at pH = 2 and 318 K and boundary between the first and second curves in 0.2 mM of DC at pH = 2 and 328 K obtained from the KASRA model disappeared which showed that in average the adsorption character of these regions were similar to each other. Also, boundary between regions of 1 and 2 of the first curve in 0.1 mM of DC at pH = 2 and 318 K (obtained from the KASRA model) disappeared and the boundary of the first and second curves moved toward smaller time which showed the character of these two curves was similar to the second curve. In these three recent cases, boundaries disappeared and characters of those regions became similar to each other due to a decrease in DC concentration and an increase in temperature.

In 0.1 M NaCl of 0.2 mM of DC at pH = 2, inconsistent with ideal results obtained from the KASRA model, there were no boundaries between the first and second curves which showed these regions were similar to each other.

At pH=2 at 70 rpm, boundaries of the first and second curves moved to smaller times compared to those obtained from the KASRA model which showed that properties of their boundaries were more similar to region 2a than region 2b.

3. 4. Using GO/PAMAM4 for Selective Separation of Metal Ions and Tannic Acid

In a series of tests, it was observed that some metal ions, including Pb^{2+} , Cr^{3+} and Cd^{2+} and also tannic acid (TA) were not adsorbed by GO/PAMAM4 and was used for separation of them from DC ions. These tests were carried out at pH = 2 which resulted in a highly positively

charged surface of GO/PAMAM4 that adsorbed severely DC ions and repelled the positively charged metal ions. Concentrations of Pb²⁺, Cr³⁺ or Cd²⁺ ions in mixed solutions of these ions with DC before and after adding adsorbent to the solutions were measured by the Agilent 200 series AA atomic absorption spectrophotometer and it was observed that only DC ions were adsorbed on GO/ PAMAM4. We used mixed solutions of 0.025 mM of DC and 0.01 mM of each of above-mentioned ions and 0.006 g of adsorbent at pH = 2. For example, the UV spectra of this process for selective separation of Cr³⁺ from its mixture with DC were shown in Fig. 13. Also, GO/PAMAM4 was used to separate DC from tannic acid (TA), Fig. 14. pK_a of TA^{68} is nearly 6 and at pH = 2, its phenolic hydroxyl groups did not dissociate and thus was not negatively-charged and did not have affinity to be adsorbed on GO/PAMAM4. As seen from Fig. 15, due to adsorption of DC on GO/

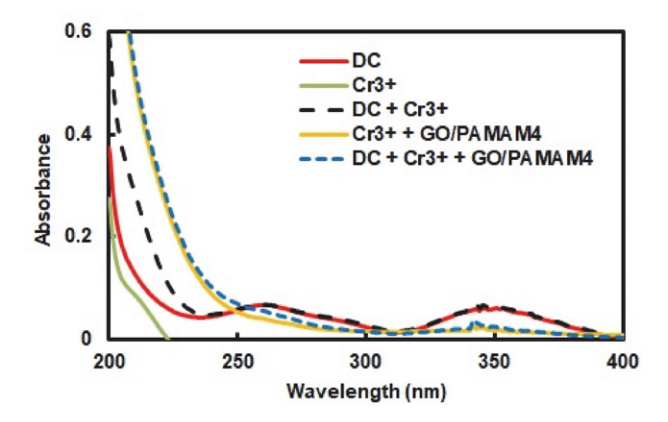


Fig. 13. UV-Vis spectra of (1) 0.025 mM DC, (2) 0.01 mM $\rm Cr^{3+}$, (3) 0.025 mM DC + 0.01 mM $\rm Cr^{3+}$, (4) 0.01 mM $\rm Cr^{3+}$ + 0.006 g GO/ PAMAM4 and (5) 0.025 mM DC + 0.01 mM $\rm Cr^{3}$ + 0.006 g GO/ PAMAM4. The volume of solution in each bottle was 10 mL. In all solutions pH was 2 and tests were carried out at room temperature and during one hour

Fig. 14. Tannic acid structure

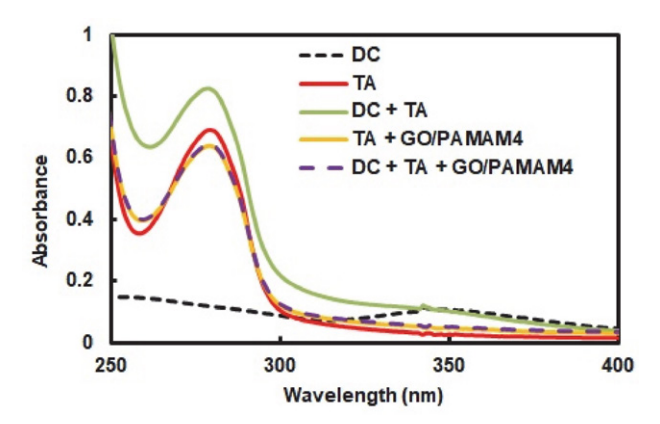


Fig. 15. UV spectra of (1) 0.025 mM DC, (2) 0.05 mM TA, (3) 0.025 mM DC + 0.05 mM TA, (4) 0.05 mM TA + 0.006 g GO/PAMAM4 and (5) 0.025 mM DC + 0.05 mM TA + 0.006 g GO/PAMAM4. pH of all solutions was 2 and tests were carried out at room temperature and during one hour. The volume of solution in each bottle was 10 mL

PAMAM4, TA was separated completely from DC ions. Some practical applications of separation of metal ions and TA⁶⁹ were explained in supporting information.

3. 5. Recycling the Used GO/PAMAM4

According to results of our experiments, in alkaline pHs, DC ions changed to chromate ions and as was observed in the adsorption tests, chromate ions were not adsorbed on GO/PAMAM4, Eq. (18). Thus, for recycling the used GO/PAMAM4, in a series of experiments at room temperature, 15 mL of 0.1 M NaOH solution was added to 0.005 g used GO/PAMAM4 and after about half an hour, adsorbent was washed with distilled water and the solution turned in yellow. It was observed that after three times recycling, the adsorption capacities of the recycled GO/

PAMAM4 were about 92–95% of the as-synthesized GO/PAMAM4. Details of this process were explained in supporting information.

$$Cr_2O_7^{2-}...GO/PAMAM4_{(S)} + 2OH^- \rightarrow 2CrO_4^{2-} + H_2O + GO/PAMAM4_{(S)}$$
 (18)

where $Cr_2O_7^{2-}$. ..GO/PAMAM4_(S) and GO/PAMAM4_(S) were the used and recycled adsorbents, respectively.

4. Conclusions

In this research, mesoporous GO/PAMAM4 nano-compound was prepared from GO and PAMAM4 dendrimer and was used as an eco-friendly adsorbent for dichromate (DC) ions. GO/PAMAM4 had two different types of various adsorption sites which at pHs of 0, and 2 were protonated forms of primary and tertiary amine groups of GO/PAMAM4 which were shown as $-NH_3^+$ and $-NHR_2^+$, and at pHs of 3 and 6 were $-NH_3^+$ groups. DC ions interacted with these adsorption sites through electrostatic interaction. It was observed that in alkaline solutions DC ions changed to chromate ions and chromate ions were not adsorbed on the GO/PAMAM4 surface.

Due to stronger interaction of -NH₃⁺ groups and their location on the end of PAMAM4 branches of adsorbent, at pHs of 3 and 6 DC ions interacted with them and analysis of their isotherms by the ARIAN model showed that they were composed from regions I and IIA and at pHs of 0, 1 and 2 interacted first with -NH₃⁺ (composed from regions I and IIA) and then with -NHR₂⁺ groups (region IIB) which was due to opening the structure of PAMAM4 at pHs of 0-2. Study of DC adsorption on this adsorbent at pH = 2 showed that adsorption capacity for DC ions increased with an increase in temperature and the process was endothermic. Maximum capacity for adsorption of DC ions was 246.7 mg g⁻¹ at pH = 0 and 318 K.

Adsorption kinetics of DC on GO/PAMAM4 was studied by the KASRA model and intraparticle diffusion, ISO and NIPPON equations. At pHs of 3 and 6, kinetic curve was composed from regions 1 and 2 (due to adsorption on $-NH_3^+$ sites) and at pHs of 0, 1 and 2 they were formed from regions 1, 2a and/or 2b (for adsorption on $-NHR_2^+$ sites) and 2a and/or 2b (for adsorption on $-NHR_2^+$ sites). At pH = 2, adsorption accelerations and velocities of regions 1 and 2a and/or 2b of the first curve (obtained from the KASRA model) and the value of k_{I1} rate constants of region 1 (obtained from ISO equation) for adsorption of DC on $-NH_3^+$ sites increased with an increase in temperature, shaking rate and decreased with increasing ionic strength.

 k_{I1} rate constants in the range of 308–328 K obeyed from Arrhenius equation and thus adsorption in region 1 was adsorption-controlled. Analysis of kinetic data by using the NIPPON equation showed that boundaries of dif-

ferent regions of kinetic curve(s), obtained from the KAS-RA model, at pHs of 1, 3 and 6 (water) and also cases at pH of 2 and 0.2 mM of DC at 318 and 328 K at 100 rpm and 318 K at 40 rpm were ideal and similar to those obtained from the KASRA model. By using data of this research, we can find the optimum condition for separating of DC from wastewater produced in labs and also removing DC stains from surfaces and clothes by this recyclable adsorbent. Thus, during a series of tests some metal ions like Pb²⁺, Cd²⁺ and Cr³⁺ and tannic acid (TA) were separated successfully from their mixtures with DC ions. Finally, the DC-adsorbed GO/PAMAM4 was regenerated by using an alkaline solution.

Acknowledgement

The authors would like to extend their gratitude to Prof. Nahid Rahimi Fard and her team at Sarv Saadat Medical Laboratory for their collaboration on the cytotoxicity tests.

5. Reference

- M. Che Razali, N. Abdul Wahab, N. Sunar, N. Hazahsha Shamsudin, Membranes 2023, 13, 285.
 - DOI:10.3390/membranes13030285
- T. S. Algarni, A. M. Al-Mohaimeed, J. King Saud Univ. Sci. 2022, 34, Article ID: 102339.
 - DOI:10.1016/j.jksus.2022.102339
- M. Maurer, D. Abramovich, H. Siegrist, W. Gujer, Water Research 1999, 33, 484–493.
 - **DOI:**10.1016/S0043-1354(98)00221-8
- 4. M. Sillanpää, M. Chaker Ncibi, A. Matilainen, M. Vepsäläinen, *Chemosphere* **2018**, *190*, 54–71.
 - DOI:10.1016/j.chemosphere.2017.09.113
- H. Al Abdulgader, V. Kochkodan, N. Hilal, Sep. Pur. Technol. 2013, 116, 253–264. DOI:10.1016/j.seppur.2013.05.052
- J. Wang, H. Chen, Sci. Total Environ. 2020, 704, Article ID: 135249. DOI:10.1016/j.scitotenv.2019.135249
- Q. Zhang, X. Chen, Z. Zhang, W. Luo, H. Wu, L. Zhang, X. Zhang, T. Zhao, *Bioresour. Technol.* 2020, 315, Article ID: 123813. DOI:10.1016/j.biortech.2020.123813
- A. Srivastava, R. Singh, V. D. Rajput, T. Minkina, S. Agarwal, M. C. Garg, *Chemosphere* 2022, Article ID: 135230.
 DOI:10.1016/j.chemosphere.2022.135230
- 9. D. Luo, K. Haverstick, N. Belcheva, E. Han, W. M. Saltzman, *Macromolecules* **2002**, *35*, 3456–3462.
 - DOI:10.1021/ma0106346
- 10. M. Florendo, A. Figacz, B. Srinageshwar, A. Sharma, D. Swanson, G.L. Dunbar, J. Rossignol, *Molecules* **2018**, *23*, Article ID: 2238. **DOI:**10.3390/molecules23092238
- H. He, Q. Yuan, J. Bie, R.L. Wallace, P. J. Yannie, J. Wang, M. G. Lancina, O. Y. Zolotarskaya, W. Korzun, H. Yang, S. Ghosh, *Transl. Res.* 2018, 193, 13–30. DOI:10.1016/j.trsl.2017.10.008
- 12. V. Gupta, S. Nayak, J. Appl. Pharm. Sci. 2015, 5, 117-22.

- DOI:10.7324/JAPS.2015.50321
- C. Dufès, I. F. Uchegbu, A.G. Schätzlein, Adv. Drug Delivery Rev. 2005, 57, 2177–202. DOI:10.1016/j.addr.2005.09.017
- Y. Gao, J. Wang, M. Chai, X. Li, Y. Deng, Q. Jin, J. Ji., ACS Nano 2020, 14, 5686–5699. DOI:10.1021/acsnano.0c00269
- P. Tarach, A. Janaszewska, *Int. J. Mol. Sci.* 2021, *22*, Article ID: 2912. DOI:10.3390/ijms22062912
- V. Márquez-Miranda, J. Abrigo, J. C. Rivera, I. Araya-Duran, J. Aravena, F. Simon, N. Pacheco, F. D. Gonzalez-Nilo, C. Cabello-Verrugio, *Int. J. Nanomed.* 2017, *12*, 1985–1999. DOI:10.2147/IJN.S125521
- J. Lee, J.G. Jackman, J. Kwun, M. Manook, A. Moreno, E. A. Elster, A. D. Kirk, K. W. Leong, B. A. Sullenger, *Biomaterials* 2017, 120, 94–102. DOI:10.1016/j.biomaterials.2016.12.024
- Q. Zhong, O.M. Merkel, J. J. Reineke, S. R. P. Da Rocha, *Mol. Pharm.* 2016, *13*, 1866–1878.
 - DOI:10.1021/acs.molpharmaceut.6b00036
- D. A. Tomalia, H. Baker, J. Dewald, M. Hall, G. Kallos, S. Martin, J. Roeck, J. Ryder, P. Smith, *Polym. J.* 1985, *17*, 117–132.
 DOI:10.1295/polymj.17.117
- D. A. Tomalia, *Macromolecules* 1986, 19, 2466–2468.
 DOI:10.1021/ma00163a029
- J. Peterson, A. Ebber, V. Allikmaa, M, Lopp, *Proc. Estonian Acad. Sci. Chem.* 2001, 50, 156–166.
 DOI:10.3176/chem.2001.3.05
- 22. M. Ficker, V. Paolucci, J. B. Christensen, *Can. J. Chem.* **2017**, 95, 954–964. **DOI:**10.1139/cjc-2017-0108
- 23. Y. Piao, T. Wu, B. Chen, *Ind. Eng. Chem. Res.* **2016**, *55*, 6113–6121. **DOI**:10.1021/acs.iecr.6b00947
- W. S. Hummers, R. E. Offeman, J. Am. Chem. Soc. 1958, 80, 1339. DOI:10.1021/ja01539a017
- S. Movahedi, M. Adeli, A. KakanejadiFard, M. Maleki, M. Sadeghizadeh, F. Bani, *Polymer* 2013, 54, 2917–2925.
 DOI:10.1016/j.polymer.2013.04.014
- J. I. Paredes, S. Villar-Rodil, A. Martínez-Alonso, J. M. D. Tascón, *Langmuir* 2008, 24, 10560–10564.
 DOI:10.1021/la801744a
- A. M. L. Oliveira, M. Machado, G. A. Silva, D. B. Bitoque, J. T. Ferreira, L. A. Pinto, Q. Ferreira, *Nanomaterials* 2022, 12, Article ID 1149 DOI:10.3390/nano12071149
- 28. H. Sachdeva, *Green Process. Synth.* **2020**, *9*, 515–537. **DOI:**10.1515/gps-2020-0055
- M. Kowalska-Góralska, K. Czyż, Z. Dobrzański, B. Patkowska-sokoła, Z. Kowalski, *Przemysl Chemiczny* 2010, 89, 430–433.
- 30. Y. Tian, Z. Yu, L. Cao, X. Li Zhang, C. Sun, D-W Wang, *J. Energy Chem.* **2021**, *55*, 323–344.
 - DOI:10.1016/j.jechem.2020.07.006
- 31. S. Priyadarsini, S. Mohanty, S. Mukherjee, S. Basu, M. Mishra, *JNC* **2018**, *8*, 123–137. **DOI**:10.1007/s40097-018-0265-6
- 32. X. Fu, J. Lin, Z. Liang, R. Yao, W. Wu, Z. Fang, W. Zou, Z. W u, H. Ning, J. Peng, *Surf. Interfaces* 2023, *37*, 102747. DOI:10.1016/j.surfin.2023.102747
- 33. M. Saha, C.R. Srinivas, S.D. Shenoy, C. Balachandran, *Contact Dermatitis* **1993**, *28*, 260–264.
 - DOI:10.1111/j.1600-0536.1993.tb03428.x

- P. Roto, H. Sainio, T. Reunala, P. Laippala, Contact Dermatitis. 1996, 34, 43–50
 - **DOI:**10.1111/j.1600-0536.1996.tb02111.x
- M. Rafi, B. Samiey, CH Cheng, *Materials* 2018, 11, Article ID 496. DOI:10.3390/ma11040496
- 36. M. Rafi, B. Samiey, C-H Cheng, *Acta Chim. Slov.* **2020**, *67*, 1124–1138. **DOI**:10.17344/acsi.2020.5963
- O. C. Compton, D. A. Dikin, K. W. Putz, L. C. Brinson, S. B. T. Nguyen, *Adv. Mater.* 2010, 22, 892–896.
 DOI:10.1002/adma.200902069
- L. Huyck, C. Ampe, M. Van Troys, Assay and drug development technologies 2012, 10, 382–392.
 DOI:10.1089/adt.2011.391
- 39. H. S. Huang, J. F. Chiou, H. F. Chiu, Archive der pharmazie 2002, 335, 33–38.
 DOI:10.1002/1521-4184(200201)335:1<33::AID-ARD P33>3.0.CO;2-G
- 40. B. Samiey, S. Golestan, *Cent. Eur. J. Chem.* **2010**, *8*, 361–369. **DOI:**10.2478/s11532-009-0135-7
- 41. B. Samiey, S. Abdollahi Jonaghani. *J. Pollut. Eff. Con.* **2015**, 3, Article ID 2.
- 42. M. I. Themkin, Zh. Fit. Khim. 1941, 15, 296-332.
- 43. M. Ozacar, I.A. Şengil, *Colloids Surf. A* **2004**, *242*, 105–113. **DOI**:10.1016/j.colsurfa.2004.03.029
- 44. B. Samiey, S. Farhadi, Acta Chim. Slov. 2013, 60, 763-773.
- 45. B. Samiey, A. Dadkhah Tehrani, *J. Chin. Chem. Soc.* **2015**, *62*, 149–162. **DOI**:10.1002/jccs.201400093
- N. Safar Beyranvand, B. Samiey, A. Dadkhah Tehrani, K. Soleimani K, *J. Chem. Eng. Data* 2019, 64, 5558–5570.
 DOI:10.1021/acs.jced.9b00655
- 47. S. Ghobadi, B. Samiey, E. Esmaili, C-H Cheng, *Acta Chim. Slov.* **2023**, 70, 44–58. **DOI**:10.17344/acsi.2022.7777
- N. Jahan, H. Roy, A. H. Reaz, S. Arshi, E. Rahman, S. H. Firoz, Md. S. Islam, CSCEE, 2022, 6, 100239.
 DOI:10.1016/j.cscee.2022.100239
- 49. K. S. W. Sing, D.H. Everett, R. A. W. Haul, L. Moscou, R. A. Pierotti, J. Rouquerol, T. Siemieniewska, *Pure Appl. Chem.* **1985**, *57*, 603–619.
- J. Song, X. Wang, C-T Chang C-T, *J. Nanomater.* **2014**, Article ID 276143.
- X. Zheng, T. Wang, H. Jiang, Y. Li, T. Jiang, J. Zhang, S. Wang, Asian journal of pharmaceutical sciences 2013, 8, 278–286.
 DOI:10.1016/j.ajps.2013.09.001
- 52. D. M. Shadrack, E. B. Mubofu, S. S. Nyandoro, *Int. J. Mol. Sci.* **2015**, *16*, 26363–26377. **DOI:**10.3390/ijms161125956
- 53. A. Ramezanpour, K. Karami, M. Kharaziha, C. Silvestru, P. Bayat, *Appl. Organomet. Chem.* **2021**, Article ID 6329.
- X. Jiao, Y. Qiu, L. Zhang, X. Zhang, RSC Adv., 2017, 7, 52337–52344. DOI:10.1039/C7RA10809E
- Y. Zeng, Y. Kurokawa, T-T Win-Shwe, Q. Zeng, S. Hirano, Z. Zhang, H. Sone, *J. Toxicol. Sci.* 2016, 41, 351–370.
 DOI:10.2131/jts.41.351
- 56. M. A. Dobrovolskaia, A. K. Patri, J. Simak, J.B. Hall, J. Semberova, S.H. De Paoli Lacerda, S.E. McNeil, Mol Pharm. 2012 Mar 5; 9(3): 382–393. DOI:10.1021/mp200463e
- 57. W. Xiao, B. Yan, H. Zeng, Q. Liu, Carbon 2016, 105, 655-664.

- **DOI:**10.1016/j.carbon.2016.04.057
- 58. P. K. Maiti, T. Çağin, S-T Lin, W. A. Goddard, *Macromolecules* **2005**, *38*, 979–991. **DOI**:10.1021/ma049168l
- Y. Liu, V. S. Bryantsev, M. S. Diallo, W. A. Goddard, J. Am. Chem. Soc. 2009, 131, 2798–2799. DOI:10.1021/ja8100227
- F. Brito, J. Ascanioa, S. Mateoa, C. Hernandeza, L. Araujoa, P. Gili, P. Martin-Zarzab, S. Dominguez, A. Mederos, *Polyhedron*, 1997, 16, 3835–3846.
 DOI:10.1016/S0277-5387(97)00128-9
- Y. A. B. Neolaka, Y. Lawa, J. A. Naat, A. A. P. Riwu, M. Iqbal,
 H. Darmokoesoemo, H. S. Kusuma, *JMR&T*, 2020, 9, 6544–6556. DOI:10.1016/j.jmrt.2020.04.040
- 62. Z. Sun, B. Liu, M. Li, C. Li, S. Zheng, *JMR&T*, **2020**, *9*, 948–959. **DOI:**10.1016/j.jmrt.2019.11.034
- 63. C. Zu, D. Zhong, H. Chang, J. Mou, H. Wang, H. Shen, *J. Environ. Chem. Eng.*, **2022**, *10*, Article ID108977.
- R. K. Madri, D. Tiwari, I. Sinha, RSC Adv., 2021, 11, 11204– 11214. DOI:10.1039/D0RA07425J
- H. S. Ramadan, M. Mobarak, E. C. Lima, A. Bonilla-Petriciolet, Z. Li, M. K. Seliem, *J. Environ. Chem. Eng.*, 2021, 9, Article ID 105352. DOI:10.1016/j.jece.2021.105352
- 66. G-H Gwak, M-K Kim, J-M Oh, *J. Nanomater.* **2016**, *37*, 1–10. **DOI:**10.1155/2016/8032615
- 67. A. Al Shra'ah, JJC, 2020, 15, 13-22.
- W. Yan, M. Shi, C. Dong, L. Liu, C. Gao, Adv. Colloid Interface Sci. 2020, 284, 102267. DOI:10.1016/j.cis.2020.102267
- Z. Su-fang, Y. Yong, S. Shao-min, D. Chuan, Food Science 2009, 30, 218–220.

Povzetek

V študiji smo uporabili grafen oksid/poliamidoamin G4 kot biokompatibilen nanokompozitni adsorbent za adsorbcijo dikromatnih ionov. V alkalnih raztopinah so se dikromat ioni spremenili v kromatne ione, ki niso bili adsorbirani na površini adsorbenta. Tako so bili eksperimenti izvedeni v kisli in nevtralni vodni raztopini. Pri teh pogojih so bila adsorpcijska mesta adsorbenta protonirana s primarnimi in ternarnimi amino skupinami adsorbenta, prikazanimi kot $-NH_3^+$ in $-NHR_2^+$, ki so adsorbirali dikromatne ione z elektrostatsko interakcijo. Adsorpcijske izoterme dikromata na grafen oksidu/poliamidoaminu G4 so bile pridobljene pri različnih ionskih močeh, pH in temperaturah. Izoterme smo analizirali z modelom regionalne analize adsorpcijske izoterme (ARIAN). Najvišja opažena adsorpcijska kapaciteta tega procesa je bila 246,7 mg g⁻¹ pri pH = 0 in 318 K. Testi pri pH = 2 so pokazali, da je ta proces endotermen. Adsorpcijski kinetični eksperimenti so bili izvedeni pri različnih začetnih koncentracijah dikromata, pH, temperaturah, hitrostih stresanja in ionskih močeh ter analizirani s kinetiko študije adsorpcije v regijah s konstantnim adsorpcijskim pospeševalnim modelom (KASRA) in difuzijo delcev, z enačbo idealno-sekundarnega reda (ISO) in neidealnim procesom adsorpcijske kinetike (NIPPON). Štiriregijska modela ARIAN in KASRA z uporabo serije enačb lahko interpretirata termodinamiko in kinetiko interakcij adsorbenta in adsorbata pri različnih pogojih. Pb^{2+,} Cd^{2+,} Cr³⁺ in taninske kisline smo ločili z grafen oksidom/poliamidoaminom G4 z alkalno raztopino.



Except when otherwise noted, articles in this journal are published under the terms and conditions of the Creative Commons Attribution 4.0 International License